Acta Crystallographica Section B
Structural Science
ISSN 0108-7681

Dynamic orientational disorder in crystals of fluoroelpasolites, structural refinement of $(NH_4)_3AlF_6$, $(NH_4)_3TiOF_5$ and Rb_2KTiOF_5

Anatoly A. Udovenko* and Natalia M. Laptash

Institute of Chemistry, Far Eastern Branch of RAS, Pr. Stoletiya 159, Vladivostok 690022, Russian Federation

Correspondence e-mail: udovenko@ich.dvo.ru

Received 13 August 2011
Accepted 26 October 2011

Dedicated to our untimely deceased colleague Vladimir A. Davydov.

Room-temperature crystal structures of triammonium hexafluoroaluminate, $(NH_4)_3AlF_6$ (I), and triammonium oxopentafluorotitanate, $(NH_4)_3TiOF_5$ (II), were refined, and the crystal structures of dirubidium potassium oxopentaflourotitanate, Rb_2KTiOF_5, at 297 K (III) and 218 K (IV) were determined using single-crystal X-ray diffraction techniques. In ammonium fluoroelpasolites [(I) and (II)], the ligand (O, F) atoms are located in the mixed 24*e* + 96*j* position of the *Fm*3*m* unit cell. The 24*e* position is occupied by the ligand atoms predominantly in (III) and fully in (IV). 'Ordered' N1 and Rb atoms are tetrahedrally displaced from the 8*c* position into the 32*f* site, and the H atoms of the disordered ammonium group N2 are statistically distributed in the 96*k* and 32*f* positions. The Ti atoms in (II) and (IV) are shifted from the 4*a* position to 24*e* thus allowing identification of the O and F atoms in the octahedron on a local scale. The disorder in the crystals is of a dynamic nature. Unique Raman spectra of Rb_2KTiOF_5 under the laser beam of 1064 nm indicate fast octahedral reorientations resulting in physical equalizations of the Ti—O and Ti—F distances as well as in the appearance of totally synchronous Ti—O and Ti—F stretching vibrations at 750 cm^{-1}. This phenomenon is assumed to also take place under X-rays.

1. Introduction

The elpasolite structural type is widespread among inorganic fluoro- or oxofluoro complexes, $A_2BMO_xF_{6-x}$ (A and B are monovalent cations; $A > B$; x = 0–3). The classical elpasolite structure comprises cation A in the 8*c* position (coordination number, CN, is 12), cation B in the 4*b* position (CN = 6), metal atom M in the 4*a* position, and ligand atoms (O, F) in the 24*e* positions of the *Fm*3*m* unit cell (Z = 4). In most cases, the elpasolite-like structures were solved according to the above approach. Upon cooling, cubic elpasolites undergo phase transitions of different types and sequence orders (Flerov *et al.*, 1998). These transitions are frequently accompanied by small entropy changes ($\Delta S \simeq 0.1R$) and are considered to be phase transitions of a displacive type. However, rather large entropy changes [ΔS = (2.33–2.99)R] are observed for ammonium fluoroelpasolites $(NH_4)_3M^{3+}F_6$ (M^{3+} = Al, Ga, Cr, V, Fe, Sc, In) during phase transitions from cubic to triclinic low-temperature modifications (Flerov & Gorev, 2001; Flerov *et al.*, 2002). Similar phase transitions are characterized as being of the order–disorder type and connected with the orientational disorder of both $[MF_6]^{3-}$ octahedra and $[NH_4]^+$ tetrahedra. The model of such phase transitions was suggested for the first time by Moriya *et al.* (1977), and is based on two

Table 1
Experimental details.

For all structures: Cubic, $Fm\bar{3}m$, $Z = 4$. Experiments were carried out with Mo $K\alpha$ radiation using a Bruker P4 diffractometer. Absorption was corrected for by multi-scan methods, *SADABS* (Bruker, 1999). Refinement was with 0 restraints.

	(I)	(II)	(III)	(IV)
Crystal data				
Chemical formula	$H_{12}N_3AlF_6$	$(NH_4)_3TiOF_5$	$Rb_2KTiO_2F_5$	$Rb_2KTiO_2F_5$
M_r	195.11	213.03	368.94	368.94
Temperature (K)	297	297	297	218
a, b, c (Å)	8.9378 (2), 8.9378 (2), 8.9378 (2)	9.1144 (6), 9.1144 (6), 9.1144 (6)	8.9002 (1), 8.9002 (1), 8.9002 (1)	8.8879 (2), 8.8879 (2), 8.8879 (2)
V (Å^3)	713.99 (3)	757.15 (9)	705.02 (1)	702.10 (3)
D_x (Mg m^{-3})	1.815	1.869	3.476	3.490
μ (mm^{-1})	0.34	1.17	15.55	15.61
Crystal size (mm)	0.30 × 0.30 × 0.30	0.32 × 0.26 × 0.20	0.28 × 0.25 × 0.20	0.35 × 0.25 × 0.25
Data collection				
T_{min}, T_{max}	0.905, 0.905	0.706, 0.800	0.098, 0.147	0.074, 0.112
No.of measured, independent and observed [$I > 2\sigma(I)$] reflections	4547, 138, 137	4778, 149, 149	5318, 198, 138	4779, 155, 130
R_{int}	0.016	0.020	0.029	0.030
Refinement				
$R[F^2 > 2\sigma(F^2)]$, $wR(F^2)$, S	0.028, 0.076, 1.09	0.021, 0.062, 1.16	0.021, 0.073, 1.19	0.023, 0.061, 1.33
No. of reflections	137	149	138	130
No. of parameters	15	18	16	12
H-atom treatment	H-atom parameters not refined	H-atom parameters not refined	–	–
$\Delta\rho_{max}$, $\Delta\rho_{min}$ (e Å^{-3})	0.24, −0.36	0.17, −0.25	0.75, −1.07	1.09, −0.84

Computer programs used: *SMART* (Bruker, 1998), *SAINT* (Bruker, 2000), *SHELXTL* (Sheldrick, 2008).

orientations of the disordered ammonium group in the 4*b* position and eight orientations of the regular rigid octahedron with disordered ligands in the general 192*l* position. The total entropy change connected with both octahedral and tetrahedral ordering could be given as $\Delta S = R\ln 8 + R\ln 2 = R\ln 16$. This value (23.05 J K^{-1} mol^{-1}) is in close agreement with the experimental value (24.8 ± 1.9 J K^{-1} mol^{-1}) for $(NH_4)_3FeF_6$. The ΔS data obtained for a series of ammonium elpasolites $(NH_4)_2NH_4M^{III}F_6$ (M = Al, V, Cr, Fe, Ga; Tressaud *et al.*, 1986) are in accordance with the suggested model. The structural determination of $(NH_4)_3GaF_6$ by Schwarzmann (1964) indicated the 192*l* (x,y,z) ligand position as being preferable. Nevertheless, the recent MAS NMR investigation of $(NH_4)_3GaF_6$ (Krahl *et al.*, 2008) showed the incorrectness of this position.

In fact, the ligand atoms in ammonium fluoroelpasolites are statistically distributed in two, 24*e* and 96*j*, positions. The preference of this 'mixed' (or 'split') position relative to others was discussed in our previous papers (Udovenko *et al.*, 2003; Udovenko & Laptash, 2008*a*). Moreover, we found the ammonium ions at 4*b* sites to be disordered having eight possible orientations instead of two (Udovenko & Laptash, 2008*a*,*b*).

In this work we continue to refine the crystal structure of ammonium fluoroelpasolites compared with that of alkali metal fluoroelpasolite, Rb_2KTiOF_5.

2. Experimental

2.1. Synthesis

Ammonium oxofluorotitanate $(NH_4)_3TiOF_5$ was synthesized in the form of well faceted octahedral single crystals as a result of the ammoniac hydrolysis of the hot aqueous solution of $(NH_4)_2TiF_6$ with an excess of NH_4F using the original method described earlier (Laptash *et al.*, 1999). This compound served as a precursor for producing the rubidium-potassium oxofluorotitanate according to the reaction

$$(NH_4)_3TiOF_5 + Rb_2CO_3 + KF = Rb_2KTiOF_5 + 3NH_3 + CO_2 + HF + H_2O.$$

A mixture of starting materials in stoichiometric proportions was thoroughly ground, placed in a closed platinum crucible and heated at 873 K for 2 h. The cake was reground, calcined again for half an hour and quenched to room temperature. To prepare single crystals of Rb_2KTiOF_5, the powder sample was melted in a resistance furnace at 1273 K for 2 h in a nitrogen-filled glove box. The sample was then cooled down to 873 K for 20 h and quenched to room temperature by switching off the heating. The resulting colorless ball-, pellet-, prism-shaped or formless single crystals of Rb_2KTiOF_5 were used for structural determinations.

Transparent well shaped octahedral single crystals of $(NH_4)_3AlF_6$ were obtained from the fluoride aqueous solution

Table 2
Results of structural refinement of (I)–(IV).

Schemes of refinement	R_1(ANIS); s.o.f. F $(NH_4)_3AlF_6$	R_1(ANIS); s.o.f. F $(NH_4)_3TiOF_5$	R_1(ANIS); s.o.f. F Rb_2KTiOF_5 (297 K)	R_1(ANIS); s.o.f. F Rb_2KTiOF_5 (218 K)
N1(Rb) (8*c*); N2(K) (4*b*); *M* (4*a*); F(24*e*)	0.0713	0.0659	0.0282	0.0310
F (24*e* + 96*j*)	0.0465	0.0392	0.0239	0.0310
	F1 0.3333	F1 0.3333	F1 0.68 (7)	1
	F2 0.1666	F2 0.1666	F2 0.08 (7)	0
H1(32*f*), H2(96*k*), H3(32*f*)	0.0298	0.0232	–	–
N1(Rb) (32*f*)	0.0277	0.0207	0.0209	0.0260
M (24*e*)	–	0.0195	–	0.0236
X = F + O	–	0.0210	0.0208	0.0229

Table 3
Selected distances (Å) and angles (°) for (I)–(IV).

$(NH_4)_3AlF_6$			
Al—F1	1.762 (3) × 2	F1—F2	2.507 (2) × 8
Al—F2	1.784 (3) × 4	F2—F2*A*	2.523 (4) × 4
Al—Al′	–	N1—N1′	0.238 (7) × 6
F1—Al—F2	90 × 8	F2—Al—F2*A*	90 × 4
F1—Al—F1*A*	180	F2—Al—F2*B*	180 × 2
$(NH_4)_3TiOF_5$			
Ti—O1	1.695 (3)	*X*1†—F2	2.649 (2) × 8
Ti—F1	2.017 (3)	F2—F2*A*	2.673 (3) × 4
Ti—F2	1.897 (3) × 4		
Ti—Ti′	0.228 (2) × 12	N1—N1′	0.251 (8) × 6
O1—Ti—F2	94.9 (1) × 4	O1—Ti—F1	180
F1—Ti—F2	85.1 (1) × 4	F2—Ti—F2*B*	170.3 (2) × 2
F2—Ti—F2*A*	89.6 (1) × 4		
Rb_2KTiOF_5 (room temperature)			
Ti—*X*1	1.914 (2) × 2	*X*1—*X*2	2.677 (5) × 8
Ti—*X*2	1.872 (3) × 4	*X*2—*X*2*A*	2.647 (5) × 4
Ti—Ti′	–	Rb—Rb′	0.201 (1) × 6
*X*1—Ti—*X*2	90 × 8	*X*2—Ti—*X*2*A*	90 × 4
*X*1—Ti—*X*1*A*	180	*X*2—Ti—*X*2*B*	180 × 2
Rb_2KTiOF_5 (low temperature)			
Ti—O1	1.744 (3)	Ti—F1*A*	1.915 (2) × 4
Ti—F1	2.072 (3)	F1—F1′	2.698 (3) × 12
Ti—Ti′	0.232 (3) × 12	Rb—Rb′	0.201 (2) × 6
O1—Ti—F1*A*	94.9 (1) × 4	O1—Ti—F1	180
F1—Ti—F1*A*	85.1 (1) × 4	F1*A*—Ti—F1*C*	170.2 (1) × 2
F1*A*—Ti—F1*B*	89.6 (1) × 4		

† *X* = F(O); *A*, *B* – letters of equivalent positions of ligand atoms (O, F) according Fig. 5.

(Udovenko *et al.*, 2003). According to the chemical analyses of the complex, its real composition was $(NH_4)_3Al(OH)_xF_{6-x}$ (x = 0.2). We used this stoichiometric formula because it seemed impossible to distinguish between OH^- and F^- (statistically distributed in the crystal lattice) by X-ray diffraction.

2.2. Crystallographic determination

Selected single crystals of $(NH_4)_3AlF_6$ (I), $(NH_4)_3TiOF_5$ (II) and Rb_2KTiOF_5 [(III) and (IV)] were mounted on a glass fiber with epoxy resin. Data collections were carried out at 297 [for (I), (II) and (III)] and 218 K [for (IV)] using Mo $K\alpha$ radiation (λ = 0.71073 Å) on a Bruker SMART-1000 CCD diffractometer. ω-scans of 0.2° were performed at three φ settings with $2\theta = -31$ and $-60°$ at a detector distance of 45 mm with an exposure time of 20 s per frame by groups of 906 frames. All reflections were indexed in the corresponding unit cells. More details on the data collection and reduction are given in Table 1.[1] The data collection, reduction and refinement of the lattice parameters were performed using *SMART* and *SAINT-Plus* programs (Bruker, 1998, 2000). All the calculations were performed using *SHELXTL*/*PC* (Sheldrick, 2008). The structures were solved by direct methods and refined against F^2 by the full-matrix least-squares method (LSM) with anisotropic approximation of the non-H atoms.

The H1 (the tetrahedron around N1) and H2 atoms (the octahedron around N2) were primarily localized in structures (I) and (II) from the residual electron-density maps. Their coordinates were subsequently calculated according to N1 displacement and following the possible models of H arrangement around N2. Information on the structure determinations is summarized in Table 1. The scheme of structural refinements is shown in Table 2. Selected bond distances and angles are given in Table 3. Hydrogen-bond parameters are presented in Table 4.

2.3. Spectroscopic measurements

Mid-IR (400–4000 cm^{-1}) spectra were collected in Nujol mulls using a Shimadzu FTIR Prestige-21 spectrometer operating at 2 cm^{-1} resolution. FT-Raman spectra of the compounds were recorded with a RFS 100/S spectrometer. The 1064 nm line of an Nd:YAG laser (130 mW maximum output) was used for excitation of the samples. The spectra were recorded at room and low temperatures. The TriVista 577 spectrometer equipped with an Ar–Kr laser emitting at 514.5 nm was also used for recording the Raman spectra of the Rb_2KTiOF_5 single crystal at room temperature. The spectral resolution was 2 cm^{-1} at the excitation line.

3. Results and discussion

3.1. Crystal structures

The room-temperature structures of $(NH_4)_3AlF_6$ (I), $(NH_4)_3TiOF_5$ (II) and Rb_2KTiOF_5 (III) were refined assuming the symmetry space group *Fm*3*m*. Disordered elpasolite-like structure of these compounds [shown for $(NH_4)_3AlF_6$] is presented in Fig. 1. In the case of Rb_2KTiOF_5 the temperature of 218 K [structure (IV)] was chosen to be close to that of the

[1] Supplementary data for this paper are available from the IUCr electronic archives (Reference: BP5038). Services for accessing these data are described at the back of the journal.

Table 4
Hydrogen-bond parameters (Å, °) in (I) and (II).

D—H···A	D—H		H···A		D···A		D—H···A	
	(I)	(II)	(I)	(II)	(I)	(II)	(I)	(II)
N1—H11···F2	0.87	0.87	2.27	2.28	3.025 (4)	3.030 (5)	146	145
N1—H12···F2^{i}	0.87	0.87	2.17	2.18	2.896 (2)	2.899 (2)	141	140
N1—H13···F2^{ii}	0.87	0.87	2.13	2.14	2.869 (1)	2.864 (2)	142	141
N1—H14···F2^{iii}	0.87	0.87	2.03	2.03	2.794 (4)	2.786 (4)	146	145
N2—H2···F1	0.89	0.91	1.87	1.84	2.707 (3)	2.701 (3)	157	156
N2—H2···F2	0.89	0.91	1.92	1.92	2.788 (3)	2.809 (3)	164	164
N2—H2···F2^{i}	0.89	0.91	2.00	2.02	2.788 (3)	2.809 (3)	146	144

Symmetry codes: (i) z, x, y; (ii) y, z, x; (iii) $-x, z, y$.

phase transitions (215 K upon heating and 200 K upon cooling; Fokina *et al.*, 2008). The first approach was the refinement of structures (I)–(IV) using atomic coordinates obtained by direct methods (Table 2, the first line). The R_1 values for structures (I) and (II) were significantly high. Therefore, the electron-density profiles of the F atom for all structures were constructed (Fig. 2).

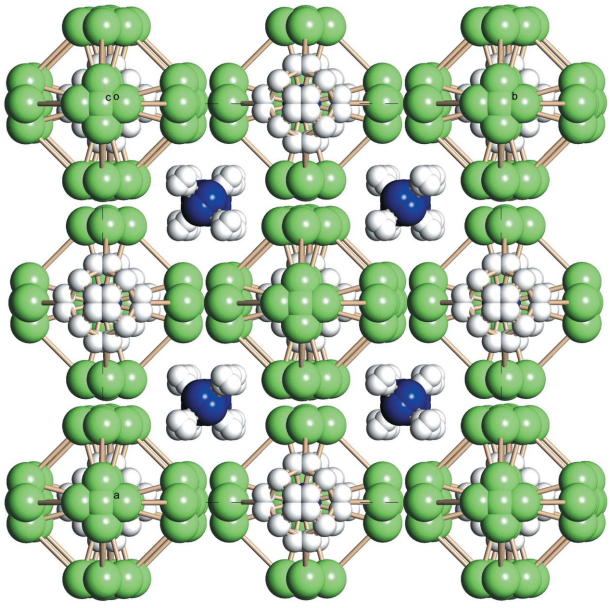

Figure 1
Disordered structure of fluoroelpasolite $(NH_4)_3AlF_6$. The green, blue and white spheres are F, N and H atoms. The central Al atoms are not seen. This figure is in colour in the electronic version of this paper.

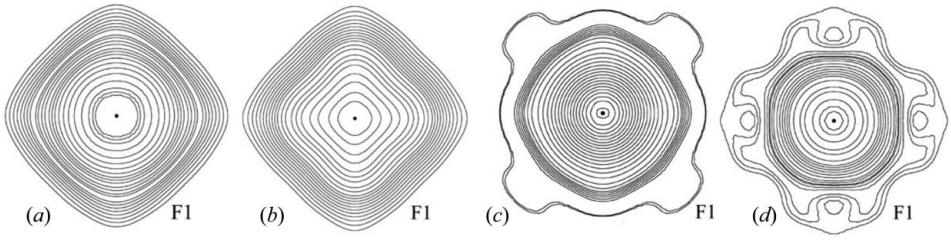

Figure 2
Electron-density distribution of the F atom in (*a*) $(NH_4)_3AlF_6$, (*b*) $(NH_4)_3TiOF_5$, (*c*) Rb_2KTiOF_5 at 293 K and (*d*) Rb_2KTiOF_5 at 218 K on the (001) plane at $z = 0.20$.

The profiles (sections) in Figs. 2(*a*) and (*b*) evidently show that the ligand (F, O) atoms in (I) and (II) occupy the 96*j* or mixed 24*e* + 96*j* position. The pure 96*j* position is not suitable since the MX_6 polyhedron in this case would be highly distorted with the XMX valent angles of 77.7–102.3° and the X—X distances of 2.24–2.76 Å. In the case of the mixed position, the MX_6 octahedron has a more acceptable geometry (Table 3). The electron-density profiles for (III) and (IV) (Figs. 2*c* and *d*) are ambiguous. The ligand atoms X in (III) also occupy the mixed position being predominantly located in the 24*e* site. The 24*e* and 96*j* sites are differently occupied in (I)–(IV). For (I) and (II), the ligand atoms of all the four octahedra of the unit cell are located in the mixed position, whereas only two octahedra in (III) have a mixed position. All the ligands in (IV) are located in the 24*e* site, since the occupation of 96*j* during the least-squares (LS) process becomes equal to 0.01 (1), and the F2 ellipsoids are badly determined (U^{11} = 0.00001, U^{22} = 0.30314, U^{33} = 0.02536 Å^2). The R_1 value had been decreased considerably for (I) and (II) and appreciably for (III) (Table 2, the second line) after the mixed 24*e* + 96*j* position was taken into account.

It should be noted that the structural peculiarities of Rb_2KTiOF_5 depended on each single-crystal sample and its 'history': whether a crystal was under X-ray exposure before the data acquisition or not. Structures (III) and (IV) were determined on different crystals at corresponding temperatures. After completing the room-temperature data collection, the same crystal was cooled down to 128 K, and structure (III) transformed into structure (IV). After heating the crystal to room temperature, structure (IV) changed into (III), but with virtually 'zero' occupation of $X2$ [0.01 (1)]. Accordingly, the F(O) and Ti electron-density profiles changed, and the corresponding structural parameters were slightly different.

At this stage of the refinement, the residual electron-density maps fixed some peaks in (I) and (II), which were located near the N atoms at a height of 0.45–0.57 e Å^{-3} with N1—Q1 distances of 0.749 for (I) [0.824 Å for (II)] and N2—$Q2$ of 0.710 (0.772 Å). These points form a tetrahedron around N1 and an octahedron around N2 corresponding to the H atoms of ordered $N1H_4$ and disordered $N2H_4$ groups. The R_1 value decreased considerably after the H atoms were added. The coordinates of the H atoms were then shifted by consecutive approximation to reasonable N—H bond lengths (0.86 and 0.89 Å). Due to this procedure R_1 was slightly decreased. Three most reasonable models of the $N2H_4$ reorientations in (I) and (II) were considered according to Seymour & Pryor (1970). We carried out a similar analysis before for the case of $(NH_4)_3MO_3F_3$ (M = Mo, W; Udovenko & Laptash, 2008*a*).

3.1.1. Model *A*. The H2 atoms (0.555, 0.555, 0.555) form a tetrahedron in two orientations bound by a twofold axis. In this case, four hydrogen bonds are formed inside

the octahedral surroundings with N2—H···F1 = 108° and N2—H···F2 = 116°. These angles are not characteristic for hydrogen bonding. With regard to H2, the LSM does not change R_1 for (I), and U_{iso} of H2 is equal to 2.0 Å^2. In this model the H atoms should form a cube from Q peaks instead of an octahedron. Such a model is realised in ammonium halogenides with the CsCl structure type (NH_4Cl, NH_4Br), where the ammonium group is cubically surrounded by Cl or Br atoms with hydrogen-bonding distances of 3.358 and 3.516 Å. The hydrogen-bonding cubic surroundings around $N2H_4$ in (I)–(II) show distances of more than 6 Å. Therefore, model *A* cannot be realised in structures (I) and (II).

3.1.2. Model *B*. The H2 atoms (0.596, 0.5, 0.5) form strong single N—H···F bonds along the coordinate axes with an angle of 180°. In this case the tetrahedron rotates freely around this bond forming six equivalent orientations. The H2 atoms form an octahedron around N2. However, the refinement of such a structure does not decrease R_1 with an approximately zero U_{iso} value (0.00001 Å^2). Thus, this model cannot be realised.

3.1.3. Model *C*. The $N2H_4$ tetrahedra form eight independent orientations. Three N2—H2 bonds deviate slightly from the coordinate axes and the fourth N2—H3 bond lies on the threefold axis. The H atoms statistically occupy two positions, 96*k* and 32*f*. Each vertex of the $N2Q_6$ octahedron is surrounded by four H2 atoms with a quadratic side of 0.34 Å. The superposition of these four H2 electron densities represents an octahedral apex (Q peak) near N2. Table 2 (line 3) presents the results of structure refinements using this model for (I) and (II). A similar model is realised in the $NH(D)_4I$ structure (structural type of NaCl) and is well described by Paasch *et al.* (1996).

The next stage of the structural refinement consists of electron-density profile constructions of N1(Rb) (Fig. 3) and N2(K) (Fig. 4). Figs. 3(*a*) and (*b*) show that the N1 atom is tetrahedrally shifted from the 8(*c*) position. The N1 displacement in (I) proceeds perpendicularly to the N—H···F hydrogen bond, and the N_4 and $N1H_4$ tetrahedra are rotated 90° relative to each other around the *c* axis. The Rb atom in (III) is also tetrahedrally displaced perpendicular to the ionic Rb—F bond (Figs. 3*c* and *d*). In the N1 sections electron density from the N—H bonds in the form of 'wings' is evident, whereas it is absent in the Rb sections. The N1(Rb) electron-density profiles in (II) and (IV) are principally the same as described above for (I) and (III). The N—N and Rb—Rb displacements in the tetrahedra are 0.238 (7) and 0.251 (8) Å for (I) and (II), and 0.201 (2) Å for (III) and (IV). The results of the structural refinement with the displaced N1(Rb) atoms are given in Table 2 (the line 4).

As seen from the N2(K) electron-density profiles (Fig. 4), the N2 external electrons are disordered over an octahedron (Figs. 4*a* and *b*), whereas the K electron density in (III) is spherical but only slightly disordered over an octahedron in (IV). The structural refinements of (I) and (II) with the disordered N atoms virtually do not alter R_1, and the two displacement anisotropic parameters in (IV) are close to zero.

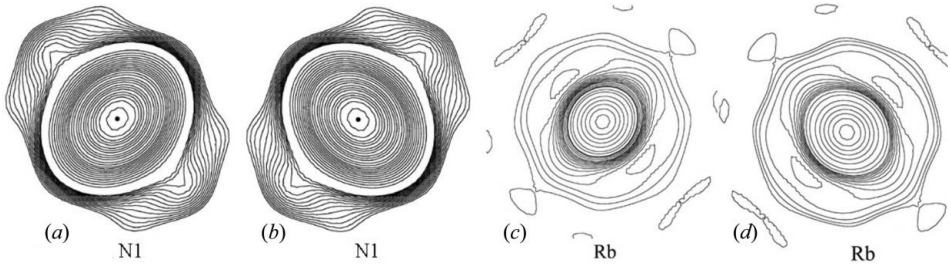

Figure 3
Electron-density distribution of N1 in $(NH_4)_3AlF_6$ (*a*) and (*b*), and Rb in Rb_2KTiOF_5 at 293 K (*c*) and (*d*) on the (001) plane at z = 0.22 and z = 0.28.

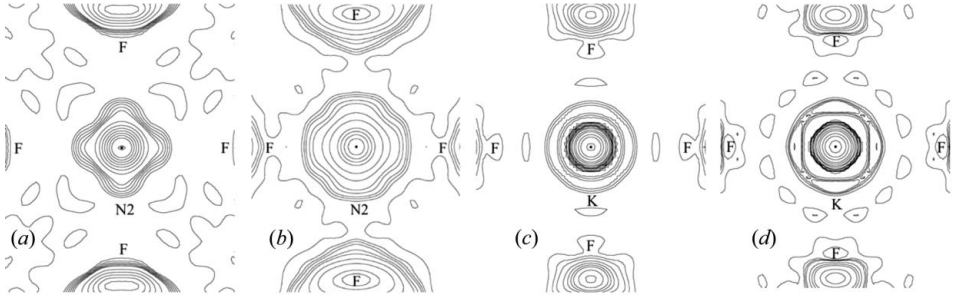

Figure 4
Electron-density distribution of N2 and K in (*a*) $(NH_4)_3AlF_6$, (*b*) $(NH_4)_3TiOF_5$, (*c*) Rb_2KTiOF_5 at 293 K, and (*d*) Rb_2KTiOF_5 at 218 K on the (001) plane at z = 0.5.

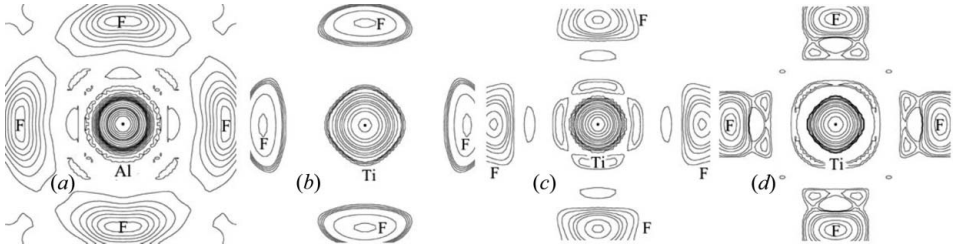

Figure 5
Electron-density distribution of Al and Ti in (*a*) $(NH_4)_3AlF_6$, (*b*) $(NH_4)_3TiOF_5$, (*c*) Rb_2KTiOF_5 at 293 K and (*d*) Rb_2KTiOF_5 at 218 K on (001) plane at z = 0.

Table 5
Vibrational frequencies for Rb_2KTiOF_5 and assignments for $[TiOF_5]^{3-}$ (C_{4v}).

Experimental (room-temperature; cm^{-1})	Calculation (cm^{-1})	Symmetry type	Assignments	Description of assignments
897	922	A_1		ν(TiO)
471	522	E		$\nu_{as}(TiF_2)$
451	491	A_1		$\nu_s(TiF_4) + \nu(TiF')$
357	378	B_2		$\nu(TiF_4)$
323	352	E		$\delta(TiOF_2)$
302	346	A_1		$\gamma(TiF_4) + \nu(TiF')$
286	305	E		$\delta(TiF_2F') + \delta(TiF_2)$
259	284	A_1		$\nu(TiF') + \gamma(TiF_4)$
205	255	B_1		$\delta(TiF_4)$
157	186	B_2		$\delta(TiF_4)$
136	149	E		$\delta(TiOF_2) + \delta(TiOF')$

Calculation: GAMESS, DFT (B3LYP) with the 631-G basis for Ti and 6311-G for light atoms (O, F).

Al and Ti electron-density profiles were also constructed in (I)–(IV) (Fig. 5). The Al and Ti atoms in (III) do not escape the 4*a* position, whereas the Ti atom is octahedrally shifted in (II) and (IV). The corresponding structural refinements confirm these conclusions. The displaced Al and Ti atoms in (III) return to the initial 4*a* position during the LSM process, whereas the Ti atom is reliably fixed in the 24*e* site for (II) and (IV). The corresponding results are presented in Table 2 (the line 5). Owing to the Ti escape from the octahedral center, the O and F atoms can be identified in a separate orientation by the Ti—*X* distances. The local structure of MX_6 polyhedra in (I)–(IV) is shown in Fig. 6 and the geometries are given in Table 3.

During the final stages of the structural refinement of (II)–(IV), the O atom was taken into account in accordance with the local geometry of the $TiOF_5$ anion, where the O ligand should occupy an *X*1 apex in (II). In (III) it is placed in the *X*1 position as well as in *X*2, which is corroborated by the shortened Ti—*X*2 distance (1.87 Å) relative to Ti—*X*1 (1.91 Å). The corresponding LSM results are presented in Table 2 (the line 6). Within error limits, R_1 slightly increased for (II) and slightly decreased for (III) and (IV). The other variants of the O arrangement were tested in (II) which resulted in an increase in R_1.

The H coordinates of the $N1H_4$ group were calculated in accordance with the tetrahedral disordering of the N1 atom displaced from the 8*c* position into the 32*f* site. The $N1H_4$ groups in (I) and (II) are shifted in parallel to each other, taking the same spatial orientation. The H atoms were fixed in the structures and were not refined by LSM. The H atoms of the two ammonium groups in (I) and (II) form strong hydrogen bonds with the F(O) atoms (Table 4). Thus, a disorder of $N1H_4$ groups or Rb cations has a displacive character, while the dynamically disordered MX_6 octahedra and $N2H_4$ tetrahedra contribute

Thus, N2 and K are not shifted from the 4*b* position ($\frac{1}{2}, \frac{1}{2}, \frac{1}{2}$) in structures (I)–(IV). The observed octahedral diffusiveness of electron density on the N atoms is, probably, the N—H electron density bond.

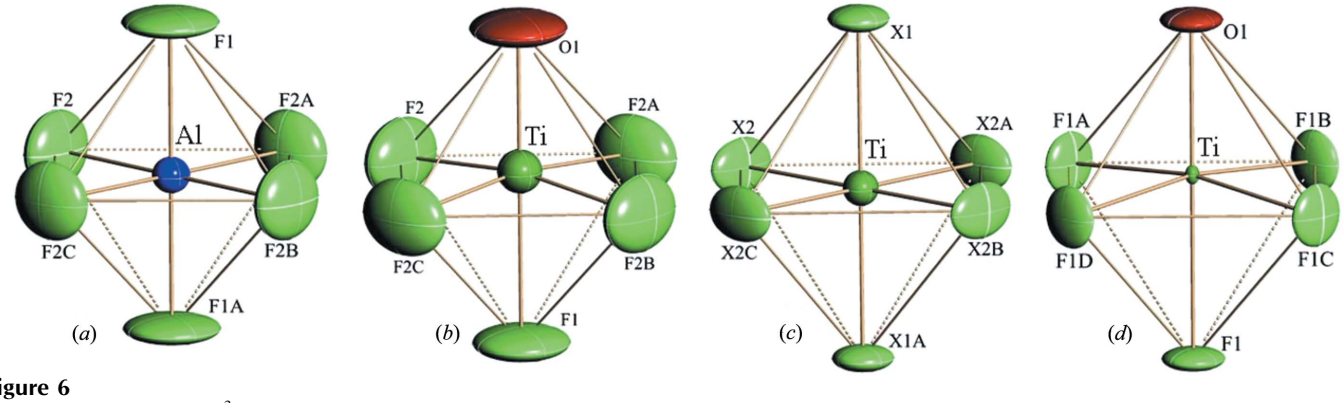

Figure 6
Local structures of $[MX_6]^{3-}$ in (I)–(IV).

mainly to the entropy changes at phase transitions which are of the order–disorder type. The dynamic nature of the latter disorder was confirmed by the ^{19}F and ^{1}H NMR investigations (Kavun, Kozlova, Laptash, Tkachenko & Gabuda, 2010).

The well pronounced first-order phase transitions with approximately equal ΔS ($\sim R\ln 8$) values were observed in $(NH_4)_3TiOF_5$ at 265 K (Flerov, Gorev, Fokina, Bovina & Laptash, 2004) and Rb_2KTiOF_5 at 215 K (Fokina *et al.*, 2008). Moreover, in the former complex the second-order phase transition at 205 K was found by ^{19}F NMR (Kavun, Kozlova, Laptash, Tkachenko & Gabuda, 2010), but not detected by the differential scanning microcalorimetry (DSM; Flerov, Fokina, Bovina & Laptash, 2004). The room-temperature phases of both compounds are characterized by a spherically symmetric (isotropic) reorientation of $[TiOF_5]^{3-}$ anions and a uniaxial reorientation of these anions in the ferroelastic phase after the phase transition. The low-temperature (LT) phase transition in $(NH_4)_3TiOF_5$ is accompanied by hindering of the uniaxial rotations of $[TiOF_5]^{3-}$ anions and a noticeable change of the ^{19}F magnetic shielding tensor associated with the influence of the pseudo-Jahn–Teller effect (Kavun, Kozlova, Laptash, Tkachenko & Gabuda, 2010). An attempt to explain the observed dynamic transformations by vibrational spectroscopy was undertaken (Voit *et al.*, 2008) using the powder sample of Rb_2KTiOF_5 obtained at 873 K. Meanwhile, in the present study, the unique Raman spectrum of Rb_2KTiOF_5 was registered under a laser beam of 1064 nm acquired on single crystals of this compound which were obtained from the melt at 1273 K.

3.2. Vibrational spectra of oxofluorotitanates

The room-temperature IR and Raman spectra of the Rb_2KTiOF_5 single crystals are presented in Fig. 7. The inconsistency between these two spectra is clearly seen. To explain the observed spectral features, a quantum-chemical calculation of vibrational spectra of the uncoordinated energy-minimized $[TiOF_5]^{3-}$ (C_{4v} symmetry) octahedral anion (claster) was performed. The results obtained are presented in Table 5. One should note that our assignments do not fully coincide with those presented elsewhere (Voit *et al.*, 2008) and accepted in the literature for $[MOF_5]^{n-}$ (Dehnicke *et al.*, 1969; Beuter & Sawodny, 1976). The main difference is that the stretching vibration of an axial F atom (F *trans* to O), ν(Ti—F′) falls in the range of the bending cluster vibrations (259_{exp}/284_{calc} cm^{-1}), which is in accordance with the ELF (electron localization function) calculations (Kavun, Kozlova, Tkachenko & Gabuda, 2010) indicating a strong ionic character of the Ti—F′ bond. The Ti—O bond has a triple character ($\sigma + 2\pi$) that ensures a rather short Ti—O distance in accordance with our structural determinations, and the Ti—O stretches lie at 870 and 897 cm^{-1} for $(NH_4)_3TiOF_5$ and Rb_2KTiOF_5, respectively. After the phase transitions these bands are split into two components, as the observed spectra of powdered samples show (Voit *et al.*, 2008). In this case, the IR and Raman spectra are correlated to each other and the calculated results.

A different situation was observed in the Raman spectrum of a single crystal of Rb_2KTiOF_5 under a laser beam of 1064 nm (Fig. 7). It can be seen that the characteristic stretches of Ti—O and Ti—F bonds become one very intensive and broad band at 750 cm^{-1}. The broader and significantly less intensive bands at 1496 and 1070 cm^{-1} can probably be assigned to its overtone and its combination with $\delta(TiOF_2)$. It should be noted, however, that under a laser beam of 514 nm, the Ti—O stretch appears in its regular place at 900 cm^{-1}. This gives the inevitable conclusion of the resonant character of the observed phenomenon. Most likely, under the laser beam of 1064 nm, a strong frequency increase of rotational $[TiOF_5]$ jumping takes place. One can assume that these jumping reorientations proceed so rapidly that the central atom does not keep pace with oxygen and remains near the symmetry center. In this case, the Ti—O and Ti—F distances should be equalized. The calculation of this state results in synchronous vibrations of Ti—O and Ti—F bonds, the highest frequency of which (totally symmetric) falls around 700 cm^{-1}. Attention should be given to the fact that this band 'reacts' to the phase transition: it is split after the phase transitions (Fig. 8) which is similar to the case of a powdered sample when the Ti—O stretch at 900 cm^{-1} is split into components.

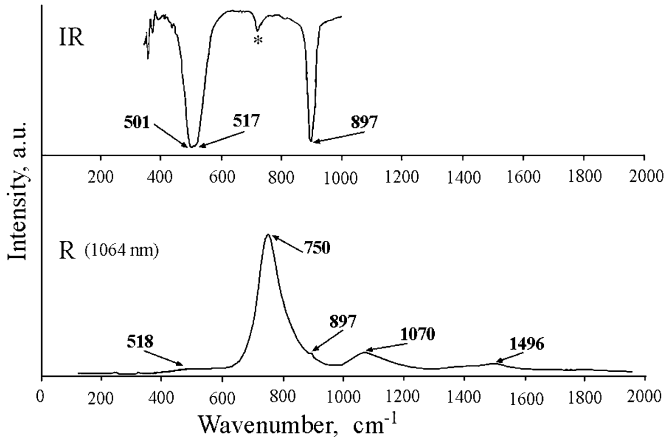

Figure 7
(IR) and Raman (laser beam 1064 nm) spectra of a single crystal of Rb_2KTiOF_5 at room temperature.

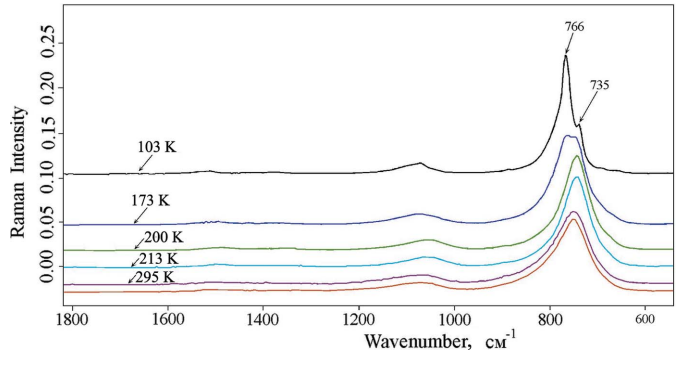

Figure 8
Temperature dependence of the Raman spectra of a single crystal of Rb_2KTiOF_5.

4. Conclusions

The electron-density profiles of all the constituent atoms allowed new features of the fluoroelpasolite structure to be found. The ligand (O, F) atoms are located mainly in the mixed 24*e* + 96*j* position of the *Fm*3*m* unit cell that ensures a tetragonal distortion of the structure after the phase transition. The $N1H_4$ groups or Rb cations are tetrahedrally shifted from the 8*c* position and disordered in the 32*f* site with the same spatial orientation. This displacive disorder does not contribute significantly to the entropy changes at the phase transitions, unlike the $N2H_4$ tetrahedra which have eight equivalent spatial orientations. These groups can remain in the center of the octahedral interstice (4*b* position), as in the cases of $(NH_4)_3AlF_6$ and $(NH_4)_3TiOF_5$, or escape into the 32*f* site, as in the case of $(NH_4)_3MO_3F_3$ (*M* = Mo, W; Udovenko & Laptash, 2008*a*). The ammonium groups and polyhedra do not move independently but form domains of lower than unit-cell symmetry, so the structural determinations of the low-temperature structure of fluoroelpasolites have so far been unsuccessful because of its polydomain character.

In fluoroelpasolites A_2BMF_6, the central atom occupies the 4*a* position of the *Fm*3*m* unit cell, whereas in oxofluoroelpasolites with ammonium cations, the central atom is displaced from the symmetry center producing either six (the case of MOF_5 octahedron) or eight (the case of MO_3F_3 octahedron) possible orientations of the anions. The O and F atoms can be identified in separate orientations owing to the inherent differences between *M*—O and *M*—F bonding. The structural refinement of $(NH_4)_3MO_2F_4$ with a possible cubooctahedral displacement of the central atom has not been found so far. Nevertheless, the escape of the central atom from the symmetry center indicates that the oxofluoro octahedron reorientation is a rigid unit. However, the case of Rb_2KTiOF_5 clearly demonstrates that the above is not always possible. The room-temperature structure of the complex shows the Ti atom remains at the symmetry center (4*a* position). Most probably, under X-rays (as well as under a laser beam of 1064 nm) jumping reorientations of the $TiOF_5$ octahedron proceed so rapidly that the central atom does not keep pace with oxygen and remains near the symmetry center. In this case the Ti—O and Ti—F distances should be equalized which is reflected in the Raman spectrum by the appearance of a 750 cm^{-1} band that is assigned to totally synchronous stretching vibrations of the Ti—O and Ti—F bonds. This intriguing phenomenon calls for further investigations.

Certainly, the order–disorder mechanism dominates in phase transitions of fluoro- or oxofluoroelpasolites but its synchronous displacive character also should not be ignored.

We thank T. B. Emelina for DFT calculations of oxofluorotitanate anions and Yu. V. Marchenko for recording the Raman spectrum of Rb_2KTiOF_5 under a laser beam at 514 nm.

References

Beuter, A. & Sawodny, W. (1976). *Z. Anorg. Allg. Chem.* **427**, 37–44.
Bruker (1998). *SMART*, Version 5.054. Bruker AXS Inc., Madison, Wisconsin, USA.
Bruker (1999). *SADABS*, Version 2.03. Bruker AXS Inc., Madison, Wisconsin, USA.
Bruker (2000). *SAINT*, Version 6.02*a*. Bruker AXS Inc., Madison, Wisconsin, USA.
Dehnicke, K., Pausewang, G. & Rüdorff, W. (1969). *Z. Anorg. Allg. Chem.* **366**, 64–72.
Flerov, I. N., Fokina, V. D., Bovina, A. F. & Laptash, N. M. (2004). *Solid State Sci.* **6**, 367–370.
Flerov, I. N. & Gorev, M. V. (2001). *Russ. Phys. Solid State*, **43**, 127–136.
Flerov, I. N., Gorev, M. V., Aleksandrov, K. S., Tressaud, A., Grannec, J. & Couzi, M. (1998). *Mater. Sci. Eng. R*, **24**, 81–151.
Flerov, I. N., Gorev, M. V., Fokina, V. D., Bovina, A. F. & Laptash, N. M. (2004). *Russ. Phys. Solid State*, **46**, 915–921.
Flerov, I. N., Gorev, M. V., Grannec, J. & Tressaud, A. (2002). *J. Fluorine Chem.* **116**, 9–14.
Fokina, V. D., Flerov, I. N., Molokeev, M. S., Pogorel'tsev, E. I., Bogdanov, E. V., Krylov, A. S., Bovina, A. F., Voronov, V. N. & Laptash, N. M. (2008). *Russ. Phys. Solid State*, **50**, 2175–2183.
Kavun, V. Ya., Kozlova, S. G., Laptash, N. M., Tkachenko, I. A. & Gabuda, S. P. (2010). *J. Solid State Chem.* **183**, 2218–2221.
Kavun, V. Ya., Kozlova, S. G., Tkachenko, I. A. & Gabuda, S. P. (2010). *Russ. J. Struct. Chem.* **51**, 463–470.
Krahl, T., Ahrens, M., Scholz, G., Heidemann, D. & Kemnitz, E. (2008). *Inorg. Chem.* **47**, 663–670.
Laptash, N. M., Maslennikova, I. G. & Kaidalova, T. A. (1999). *J. Fluorine Chem.* **99**, 133–137.
Moriya, K., Matsuo, T., Suga, H. & Seki, S. (1977). *Bull. Chem. Soc. Jpn*, **50**, 1920–1926.
Paasch, M., Mclntyre, G. J., Reehuis, M., Sonntag, R. & Loidl, A. (1996). *Z. Phys. B*, **99**, 339–344.
Schwarzmann, S. (1964). *Z. Kristallogr.* **120**, 286–316.
Seymour, R. S. & Pryor, A. W. (1970). *Acta Cryst.* B**26**, 1487–1491.
Sheldrick, G. M. (2008). *Acta Cryst.* A**64**, 112–122.
Tressaud, A., Khairoun, S., Rabardel, L., Kobayashi, T., Matsuo, T. & Suga, H. (1986). *Phys. Status Solidi A*, **96**, 407–414.
Udovenko, A. A. & Laptash, N. M. (2008*a*). *Acta Cryst.* B**64**, 305–311.
Udovenko, A. A. & Laptash, N. M. (2008*b*). *Russ. J. Struct. Chem.* **49**, 482–488.
Udovenko, A. A., Laptash, N. M. & Maslennikova, I. G. (2003). *J. Fluorine Chem.* **124**, 5–15.
Voit, E. I., Davydov, V. A., Mashkovskii, A. A. & Voit, A. V. (2008). *Russ. J. Struct. Chem.* **49**, 13–20.